PERGAMON

Applied Geochemistry 18 (2003) 719–738

Applied Geochemistry

www.elsevier.com/locate/apgeochem

Changes in isotope ratio and content of dissolved helium through groundwater evolution

Yasunori Mahara*, Toshifumi Igarashi[1]

Geology Department, Abiko Research Laboratory, Central Research Institute of Electric Power Industry, 1646 Abiko, Abiko-shi, Chiba, 270-1194, Japan

Received 22 November 2001; accepted 5 July 2002
Editorial handling by R.L. Bassett

Abstract

The dissolved He content and He isotope ratio are proxy indicators of groundwater evolution in the Shimokita peninsula. The record of ^{3}H and excess bomb tritiogenic ^{3}He reveals the intrusion depth of shallow and young groundwater into deep groundwater. The record of tritiogenic ^{3}He suggests that prior to the period of nuclear testing, the natural production level of ^{3}H irradiated by cosmic rays was probably 6 TU. Helium isotope ratios in the groundwater converge to that of the regional crustal He with increasing depth and dissolved He content. The regional degassed He has a $^{3}He/^{4}He$ (R) ratio of 7.24×10^{-7} which consists of 6% mantle He (with $R = 1.1 \times 10^{-5}$) and 94% radiogenic He (with $R = 1 \times 10^{-8}$). The magnitude of degassing He flux is 5×10^{-9} m^3/m^2 a. Based on the accumulation of He, and taking into consideration the degassing He flux, groundwater at depths greater than 300 m below sea level is estimated to be stagnant, exhibiting residence times in excess of 10^2 Ka.

1. Introduction

Groundwater contains dissolved noble gases that are equilibrated with atmospheric air. For example at 20 °C: He: 4.5×10^{-8} ccSTP/g; Ne: 1.9×10^{-7} ccSTP/g; Ar: 3.1×10^{-4} ccSTP/g; Kr: 7.2×10^{-8} ccSTP/g and Xe: 99×10^{-9} ccSTP/g (Weiss, 1971; Mazor, 1972). With the exception of He and ^{40}Ar, these noble gases are basically conserved in groundwater. The dissolved contents of Ne, Ar, Kr and Xe can provide insights into palaeotemperatures at the time groundwater was recharged (Mazor, 1972; Stute et al., 1992). In contrast, due to additions from subsurface sources, the He content is not conserved in groundwater (Andrews, 1992; Mazor and Bosch, 1992; Mahara et al., 2001; Torgersen and Clarke, 1985). Furthermore, its isotopic ratio can be changed drastically by the addition of isotopically different He components: mantle He which has a high ratio ($^{3}He/^{4}He \sim 1.1 \times 10^{-5}$) (Sano and Wakita, 1985); radiogenic He which has a low ratio ($^{3}He/^{4}He \sim 10^{-8}$), and atmospheric He which exhibits an intermediate value ($^{3}He/^{4}He \sim 1.4 \times 10^{-6}$).

For example, in Japan, He dissolved in groundwater in volcanic aquifers has a higher ratio of $^{3}He/^{4}He$ than atmospheric He, while that in crystalline rock and sedimentary rock aquifers, where there is little effect of released mantle He, has a ratio lower than that of the atmosphere (Mahara, 1995). The relation between He content and isotopic ratio indicates the stage and direction of groundwater evolution.

In this study, He content and its isotope ratio are used as a natural tracer to track groundwater in macro-circulation. The authors focused on the following topics: (1) the location of the intruding boundary of shallow groundwater into deep groundwater, (2) the level of natural ^{3}H prior to injection of man-made ^{3}H, and (3)

* Corresponding author. Tel.: +81-471-82-1181; fax: +81-471-82-5934.
E-mail addresses: mahara@criepi.denken.or.jp (Y. Mahara), toshifumi@eng.hokudai.ac.jp (T. Igarashi).
[1] Present address: Graduate School of Engineering, Hokkaido University, Sapporo, Hokkaido, 060-8626, Japan.

0883-2927/03/$ - see front matter
PII: S0883-2927(02)00177-4

the magnitude of degassing He flux and groundwater residence time of deep groundwater.

2. Study area

The study area is located in the east-central part of the Shimokita Peninsula, approximately 600 km north of Tokyo, Japan (Fig. 1). The area is on the fringe of the volcanic front line, on a plateau tableland 40–52 m above sea level. It is 2 km west of the Pacific coast, and bordered by a small river to the north and by the brackish Obuchi marsh to the south, and on the west by small, contiguous hills leading to mountains. The mountains are located approximately 10 km NW of the area and the highest peak is 560 m.

The average temperature is 8 °C and the annual precipitation is 1065 mm/a. Snow covers the ground for about 4 months in winter. The average evapotranspiration rate is estimated by Penman's method (1948) to be 400 mm/a and empirical evidence shows the average surface runoff to be 365 mm/a (Sasaki, 2000). Consequently, the net infiltration rate of rainwater into the ground was estimated to be 300 mm/a.

The area where groundwater was investigated is covered by sedimentary rocks. The surface of the area is covered with a thin Quaternary loam layer (more than 4×10^2 Ka old) which has a maximum thickness of 6 m and is composed of weathered volcanic ash. Tertiary Takahoko layers (more than 5 Ma old), consisting of tuff, sandy tuff, tuffaceous sandstone and mudstone extend from the bottom of the thin Quaternary layer to about 450 m below sea level, as illustrated in Fig. 1 (Kuroda et al., 1993).

The mudstone, tuffaceous sandstone and fine sandstone, which comprise the hydrogeological bedrock, underlie the entire area and control regional groundwater circulation. The hydraulic conductivity of the Tertiary layers is relatively low; values for mudstone and fine sandstone range from 10^{-6} to 10^{-8} cm/s and for tuffaceous sandstone, from 10^{-5} to 10^{-7} cm/s (Kuroda et al., 1993). The hydraulic conductivity measured in-situ decreases with increasing downward depth from 50 m below sea level. It is probable, therefore that deep groundwater does not move through a fracture network in this sedimentary aquifer even if fractures exist.

Deep groundwater is assumed to move very slowly, because the gradient of the groundwater total head is small and the basement rocks have low permeability. On the other hand, the water table is found a few meters below ground surface on the plateau tableland (Fig. 1). The profile of groundwater hydraulic pressure to 450 m below sea level steadily increases with depth and is approximately equivalent to that of static hydraulic pressure.

3. Materials and methods

3.1. Water sampling

Groundwater samples were collected from more than 30 wells at the site to measure ^{3}H concentrations, and the concentrations of dissolved noble gases. Volumes of the collected sample water were 1000 ml for ^{3}H concentrations, and 15 ml for dissolved noble gases. Samples were carefully collected under isolated pumping conditions at predetermined depths in wells sectioned with rubber packers (Ii et al., 1997), after pumping until pH, Eh, temperature, electric conductivity and dissolved O_2 content stabilized. The samples for determining the content of dissolved noble gases were carefully collected into annealed Cu tubes. Both ends of the Cu tubes were pinched off with steel clamps to prevent the dissolved gases from degassing and being contaminated with atmospheric air during long-term storage.

3.2. Analytical methods

The concentration of ^{3}H was measured by β-ray counting after electrolytic enrichment. 1 l of groundwater was reduced to about 40 ml by electrolysis using Ni/Fe electrodes. 40 ml of distillate and 60 ml of scintillation cocktail Aquaso-II (New England Nuclear Ltd.) were mixed in a 100-ml Teflon vial. This mixture was measured for 1000 min by a low-background liquid-scintillation counter.

The dissolved noble gases were separated from water samples in a stainless-steel extraction line under a high vacuum (1×10^{-6} mbr) with a 10-min ultrasonic vibration. A liquid-N_2 cold trap removed water vapour and condensable gases. Active gases were removed by a getter pump having 2 Ti–Zr getters, one of which was heated at 450 °C and the other was kept at room temperature. Heavy noble gases (e.g. Ar, Kr, and Xe) were removed by an activated charcoal trap cooled in liquid-N_2. Residual Ar and moisture in the purification unit were removed by cooling to 40 K by a cryogenic pump. The residual He and Ne mixture left in the purification unit was fed into a VG-5400 mass spectrometer (VG Isotopes Ltd.). First, the concentration of ^{4}He and ratios of ^{20}Ne to ^{4}He were measured 6 times in 10 min to provide 6 data sets. After cooling to 22 K by a cryogenic pump to remove Ne, the ratios of ^{3}He to ^{4}He were carefully measured at least 50 times, using a standard deviation of 1 sigma for about 60 min. The precise values of ^{4}He concentration, the ^{20}Ne^{4}He ratio and ^{3}He/^{4}He ratio were determined by comparison with two sets of standard air values which were measured under the same conditions before and after the sample was measured.

In this study, 1.384×10^{-6} was assumed as the ratio of ^{3}He/^{4}He for standard air. The ^{4}He concentration, the

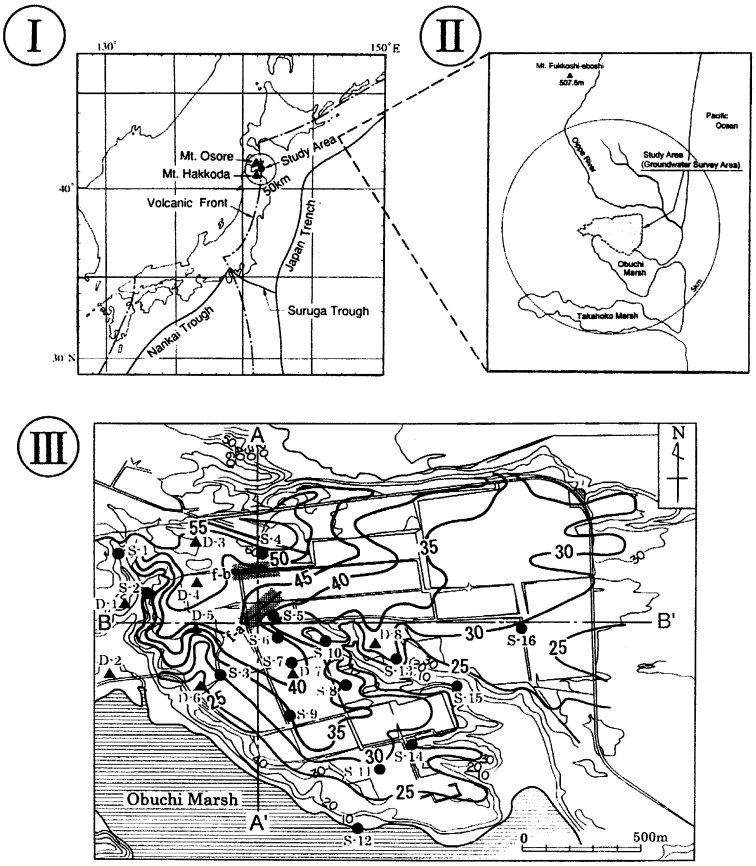

Fig. 1. (1) Location of the study area in Japan (and mutual locations within the study area, volcanic front line and active volcanic areas of Mt. Osore and Mt. Hakkoda), (II) Location of groundwater surveying area, (III) groundwater table contour map and location of groundwater sampling boreholes, and (IV) overview of vertical formation of geological layers, location of faults and water circulation and water mass balance on the site. *(—30—:* groundwater table contour level of e.g. 30 m; —30—: ground surface contour level of e.g. 30m; ●S-1–S-16: shallow wells; ⋆D-1–D-15: deep wells; A—A′ and B—B′: are vertical lines that illustrate the distribution of groundwater flow velocities and He concentration in the text).

$^3He/^4He$ ratio, and the $^{20}Ne/^4He$ ratio were determined with measurement errors of less than 0.5, 1, and 5% respectively, which were verified from the measurement reproducibility of ^4He concentrations and the ratios of $^3He/^4He$ and $^{20}Ne/^4He$ dissolved in distilled water samples. System blanks for ^4He and ^{20}Ne were 2.4×10^{-9} ccSTP and 7.2×10^{-9} ccSTP, respectively. The average gas stripping efficiency of dissolved gases from the sample water was determined to be 97% compared with that of ^4He and ^{20}Ne from samples of distilled water equilibrated with atmospheric air at 23 °C.

4. Results and discussion

4.1. Isotopic characteristics of He accumulated in groundwater

Dissolved He concentration and ratios of ^3He to ^4He and of ^4He to ^{20}Ne were measured for groundwater samples collected from 30 m above sea level to 352 m below sea level (Table 1). In order to reveal the origin of excess He accumulated in groundwater, the total He content measured in the groundwater samples were compared with the $^3He/^4He$ ratio and (He_{eq}/He_s) ratio of the He content equilibrated with atmospheric air (Fig. 2).

Shallow groundwater samples collected from the ground surface to a depth of 40 m below sea level are shown in Fig. 1. ($^3He/^4He$) and (He_{eq}/He_s) ratios exhibit a poor correlation. This is in part because the shallow groundwater has been recharged with rainwater in the past 10 a, as demonstrated by ^3H concentrations varying from hundreds of ^3H units resulting from thermonuclear tests down to natural levels. As a result, the $^3He/^4He$ ratio does not decrease systematically with the addition of crustal He. The $^3He/^4He$ ratio reaches a maximum value of 4.47×10^{-6} at the He_{eq}/He_s ratio of 0.85. Thereafter the $^3He/^4He$ ratio decreases to 1.58×10^{-6} at the He_{eq}/He_s ratio of 0.54. The maximum ratio is equivalent to the addition of excess ^3He content of 1.82×10^{-13} ccSTP/g where ^3H values of 72.9 TU decreased down towards the value of tritiogenic ^3He.

On the other hand, groundwater naturally contains only excess ^3He of 1.38×10^{-14} or 2.5×10^{-14} ccSTP/g after all ^3H turns into tritiogenic ^3He through β-decay without degassing from water if it contains a natural level of ^3H 5.5 TU (Kaufman and Libby, 1954) or 10 TU (Ravoire et al., 1970), respectively. Consequently, random variations in the $^3He/^4He$ ratio, shown in Fig. 2, were probably caused by the addition of tritiogenic ^3He from man-made ^3H injected in shallow groundwater through rainwater precipitated in the past 40 a.

Deep groundwater samples collected at depths greater than 40 m below sea level have a good correlation between the $^3He/^4He$ ratio and the He_{eq}/He_s ratio (Fig. 2-2). Data for the (He_{eq}/He_s) ratio versus the ($^3He/^4He$) ratio were least squares fitted onto a straight line through the starting point ($1.0, 1.69 \times 10^{-6}$) and the end point ($0.0, 7.24 \times 10^{-7}$) with a correlation coefficient of 0.90.

The end point ($0, 7.24 \times 10^{-7}$) on the fitted line shown in Fig. 2-2 indicates that a large amount of the crustal He component has been accumulated into groundwater circulating in strata before the (He_{eq}/He_s) ultimately reaches zero. Thus, the initial amount of atmospheric He component dissolved in groundwater can be ignored. The crustal component, which probably has a He isotope ratio ($^3He/^4He$) of 7.24×10^{-7}, is constantly and regionally supplied from mudstone in a deep bedrock floor. According to Lehmann and Loosli (1991) Φ is the neutron flux in a rock matrix and is calculated by the equation $\Phi = 10^{-5}(0.56[U] + 0.16[Th])$. As the mudstone measured at the site contained on average 2.66 ± 0.69 ppm of U, 7.30 ± 1.89 ppm of Th and 22.78 ± 3.27 ppm of Li, a rock porosity of 0.44 and a density of 2.7 g/cm^3, the radiogenic He produced in mudstone (cm^3 rock) was calculated to have a $^3He/^4He$ ratio of $7–9.5 \times 10^{-9}$. If the He dissolved in deep groundwater is produced only by the homogeneous mixing of a radiogenic He component and an atmospheric He component, the ratio of He dissolved in groundwater should reach the terminal He isotopic ratio of less than 1.0×10^{-8}. However, Fig. 2-2 suggests the He accumulated in deep groundwater has an isotope ratio of 7.24×10^{-7}. This great discrepancy indicates mixing with other He components with a high He isotope ratio.

The site that is located in the center of the Shimokita peninsula is sandwiched between two active volcanic areas shown in Fig. 1. One is Mt. Osore 40-km to the SW, and the other is Mt. Hakkoda which is located 50 km to the NW. It is not difficult to imagine that a magmatic He component with a high He isotope ratio could easily intrude into deep groundwater circulating around the site. Furthermore, this site is thickly covered by volcanic ash and various tuffaceous rocks that originated from eruption approximate 10 Ma ago. As these rocks are very porous, almost all magmatic He is probably released from rocks easily. Therefore, other sources of He which push up the He isotope ratio need to be looked for.

Although there may be still more discussion on whether or not a He component with a high He isotope ratio has been released from the rock, we have to consider at least the addition of a He component with an isotope ratio several hundred times higher than the radiogenic He produced in rocks. In addition, the magnitude of a He degassing flux in various groundwater basins in the world is summarized in Table 2. The magnitude of the ^3He flux at this site is not necessarily smaller than the contribution from mantle He to other basins. In other words, it can be assumed that a small amount of mantle He is being injected into the aquifer at the site.

The mixing ratio between these two different components can be roughly estimated by using the He isotope

Table 1
Data of dissolved noble gases (^{4}He, ^{3}He/^{4}He, ^{20}Ne/^{4}He) and ^{3}H measured in groundwater samples collected from boreholes

Borehole No.	Sampling depth (EL. m)	^{4}He×10^{-8} (ccSTP/g)	^{3}He/^{4}He × 10^{-6}	^{20}Ne/^{4}He	^{3}H (TU)	Groundwater age* (year)
(a) Shallow boreholes						
S-1	22.3	5.21±0.03	1.58±0.01	4.61	8.40±0.2	11
S-2	8.13	5.10±0.03	2.12±0.02	2.98	2.36±0.2	38
	0.13	5.25±0.03	2.14x±0.02	4.11	3.71±0.2	32
S-3	28.2	5.30±0.03	1.54±0.01	4.06	4.81±0.2	15
S-4	48.3	4.36±0.02	1.37±0.01	4.37	12.6±0.2	0
	18.3	5.72±0.03	1.28±0.01	4.50	1.60±0.2	18
S-5	18.3	5.78±0.03	1.60±0.01	3.77	25.0±0.2	6
S-6	16.0	5.24±0.03	1.70±0.01	4.14	1.52±0.2	35
	1.99	8.62±0.04	1.59±0.01	3.90	1.20±0.2	31
S-7	36.4	4.85±0.02	1.35±0.01	4.04	5.40±0.2	3
S-8	3.73	4.98±0.02	2.56±0.02	3.73	9.87±0.2	23
	−28.3	5.60±0.03	2.60±0.02	4.21	9.37±0.2	23
S-9	29.5	5.17±0.03	1.66±0.01	4.24	7.68±0.2	12
	12.5	5.75±0.03	2.14±0.02	4.19	10.0±0.2	17
S-10	−6.48	5.26±0.03	1.34±0.01	3.75	0.60±0.2	31
S-11	27.5	5.34±0.03	1.41±0.01	3.58	7.76±0.2	9
S-12	−20.8	5.42±0.03	1.94±0.02	4.10	4.05±0.2	28
S-13	24.5	4.95±0.03	2. 17±0.02	4.24	12.6±0.2	15
S-14	16.4	5.50±0.03	4.47±0.03	4.07	26.0±0.2	26
	8.37	4.62±0.02	2.51±0.02	4.74	18.0±0.2	18
	−4.63	5.68±0.03	3.82±0.03	4.21	2.0±0,2	23
S-15	−1.58	4.74±0,02	1.46±0.01	4.05	8.18±0.2	5
S-16	16.5	5.25±0,03	1.48±0.01	5.14	8.50±0.2	7
(b) Deepboreholes						
D-1	−10.5	7.61±0.05	1.22±0.009	3.06	2.8±0.2	
	−95.5	4.76±0.02	0.665±0.005	0.92	ND	
	−130.5	96.4±0.58	0.687±0.005	0.66	ND	
D-2	−22.6	7.87±0.05	1.08±0.008	2.62	1.27±0.2	
	−64.6	13.4±0.08	1.03±0.008	2.03	ND.	
	−113.0	52.4±0.31	0.55±0.004	0.55	ND.	
D-3	25.0	7.80±0.05	1.42±0.011	3.47	–	
	5.6	5.15±0.03	1.40±0.010	4.03	ND.	
	−20.0	5.62±0.03	1.37±0.010	4.61	ND.	
	−40.0	5.83±0.03	1.41±0.010	4.11	ND.	
	−60.0	7.83±0.05	1.43±0.011	3.72	ND.	
	−94.4	68.5±0.41	1.10±0.008	0.367	ND.	
	−164.4	377.0±2.26	0.637±0.005	0.06	ND.	
D-4	37.0	8.13±0.05	1.61±0.012	4.08	1.27±0.2	
	17.0	5.40±0.03	1.43±0.011	3.51	–	
	0.0	8.60±0.05	1.57±0.012	3.26	ND.	
	−50.0	5.89±0.04	1.72±0.013	4.77	ND.	
	−83.0	8.53±0.05	1.33±0.010	3.02	ND.	
	−204.0	444.0±2.66	0.575±0.004	0.06	ND.	
D-5	24.5	4.06±0.02	1.63±0.012	5.11	ND.	
	0.0	6.36±0.04	1.43±0.011	4.53	ND.	
	−45.5	5.13±0.03	1.44±0.011	4.21	ND.	
	−50.0	6.17±0.04	1.45±0.011	4.21	ND.	
	−100.0	5.95±0.04	1.37±0.010	0.42	ND.	
D-6	−9.9	5.43±0.03	2.01±0.015	4.19	1.27±0.2	
	−70.9	6.34±0.04	1.58±0.012	3.49	ND.	
	−123.9	65.1±0.39	0.796±0.006	0.48	ND.	
D-7	−3.6	7.45±0.04	1.37±0.010	4.05	–	
	−27.7	5.52±0.03	1.42±0.011	4.60	0.76±0.2	
	−54.7	6.69±0.04	1.35±0.010	2.99	ND.	
	−103.3	21.3±0.13	1.14±0.008	1.96	ND.	
	−194.7	70.7±0.42	0.781±0.006	0.25	ND.	
D-8	18.0	5.45±0.03	1.34±0.010	3.68	0.73±0.2	
	−102.0	14.4±0.09	1.16±0.009	1.63	ND.	
	−242.0	58.3±0.35	1.62±0.012	0.13	ND.	
	−352.0	1550±9.30	0.752±0.006	0.003	ND.	

ND.,under the detection limit of ^{3}H concentration (<0.2 TU); –could not analyze.

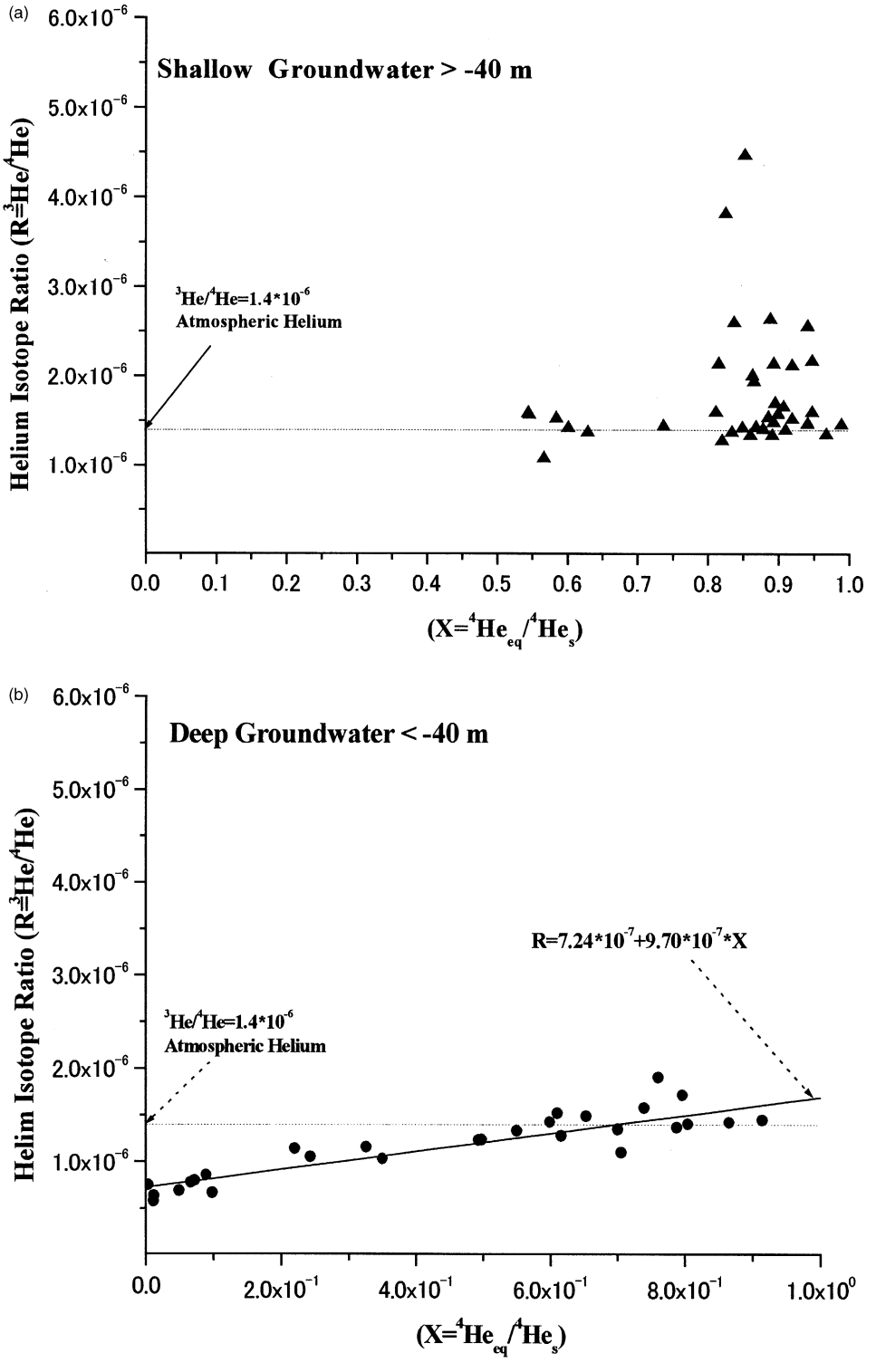

Fig. 2. Correlation between the He isotopic ratio ($^3He/^4He$) and He content ratio ($^4He_{eq}/^4He_s$) compared to the saturated He content equilibrated with atmospheric air dissolved in groundwater. Shallow groundwater is shown in Fig. 2–1 and deep groundwater is shown in Fig. 2–2. (solid triangle: shallow groundwater collected from ground surface to 40 m below sea level; solid circle: deep groundwater collected under 40 m below sea level; ^{4}Heeq: the saturated dissolved He content is 4.68×10^8 ccSTP/g when rainwater is equilibrated with atmospheric air at 8 °C which is the average temperature at the site; ^{4}He~: the total dissolved He content in samples; $R = {}^3He/{}^4He$; $X\ {}^4He_{eq}/He_s$).

Table 2
Comparison of magnitude of He degassing flux among various basins

Location of study area	^{4}He flux (atoms m^{-2} s^{-1})	^{3}He flux (atoms m^{-2} s^{-1})	Methods	References
Great Artesian Basin in Australia	8.9×10^{9}	2.7×10^{2}	Measurement in groundwater	Torgersen and Clarke (1985) Torgersen (1989)
	3.1×10^{10}	2.0×10^{3}	Estimation from in-situ data with simple model	Torgersen and Clarke (1987)
	1.8×10^{10}	–	Estimation from He transport analyses	Bethke et al. (1999)
Great Hungarian Plain	$2.5\times^{10}$	$\sim8\times10^{4}$	Measurement in groundwater	Martel et al. (1989)
	$0.7–4.5\times10^{9}$	–	Measured in groundwater and He transport analyses	Stute et al. (1992)
Paris Basin	3.8×10^{9}	3.4×10^{2}	Measurement in groundwater	Marty et al. (1993)
	7.6×10^{10}	8.3×10^{3}	Estimation from He transport analyses	Castro et al. (1998)
Molasse Basin in Austria	$2–2.6\times10^{9}$	–	Measurement and He diffusion analysis	Andrews et al. (1985)
Morsieben in Germany	$1{,}7\times10^{9}$	–	Estimation from He profile analyses	Osenbruck et al. (1998)
Auob Sandstone Aquifer in Nanubia	$1.9–2.5\times10^{10}$	–	Measurement in groundwater	Heaton (1984)
	5.1×10^{10}	–	Estimation from He transport analyses	Castro et al. (2000)
Carrizo Aquifer,Texas	3.1×10^{9}	–	Estimation from He transport analyses	
San Juan Basin, New Mexico	2.6×10^{10}	–	Estimation from He transport analyses	
Northern Taiwan, Taiwan	$2.4–2.7\times10^{10}$	$3.9\sim7.2\times10^{4}$	Measurement in gas well	Sano et al. (1986)
Kanto Plain Basin, Japan	9.6×10^{9}	1.6×10^{3}	Measurement in groundwater	Sano (1986)
Rokkasho, Japan	4.25×10^{9}	3.0×10^{3}	Estimation from He profile analyses, and He transport analyses	This study

ratio ^{3}He/$_4$He of the radiogenic He 1×10^{-8} for mudstone and that of the mantle related to various magma activities in a subduction area, 1.1×10^{-5} (Sano and Wakita, 1985, 1988). At this site, the crustal He approximately consists of a mixture of 94% radiogenic He and 6% mantle He related to volcanic activity. It can be concluded that deep groundwater at this site has largely accumulated the crustal He component with a ^{3}He/^{4}He ratio of 7.24×10^{-7}.

4.2. Characterization of the intruding shallow groundwater boundary and estimation of natural ^{3}H production level from excess ^{3}He content

The concentrations of the dissolved excess ^{3}He were calculated using the measured ^{4}He content and ^{3}He/ ^{4}He ratio. The relation between dissolved excess ^{3}He content and the sampling depth of groundwater is illustrated in Fig. 3. Systematic changes in the profile of excess ^{3}He content were observed between 40 and 50 m below sea level. After this ^{3}He concentration increases considerably with increasing sampling depth from 50 to 325 m below sea level.

It can be deduced from Fig. 2-1 that the excess ^{3}He found to a depth of 40 m below sea level was caused by the addition of tritiogenic ^{3}He resulting from manmade ^{3}H that was injected into the shallow groundwater following the thermonuclear testing era. All groundwater samples collected to a depth of 40m below sea level contain levels of ^{3}H ranging from 0.6 to 20.8 TU. In contrast, ^{3}H could no be found in any of the samples collected at depths below 50 m below sea level. The

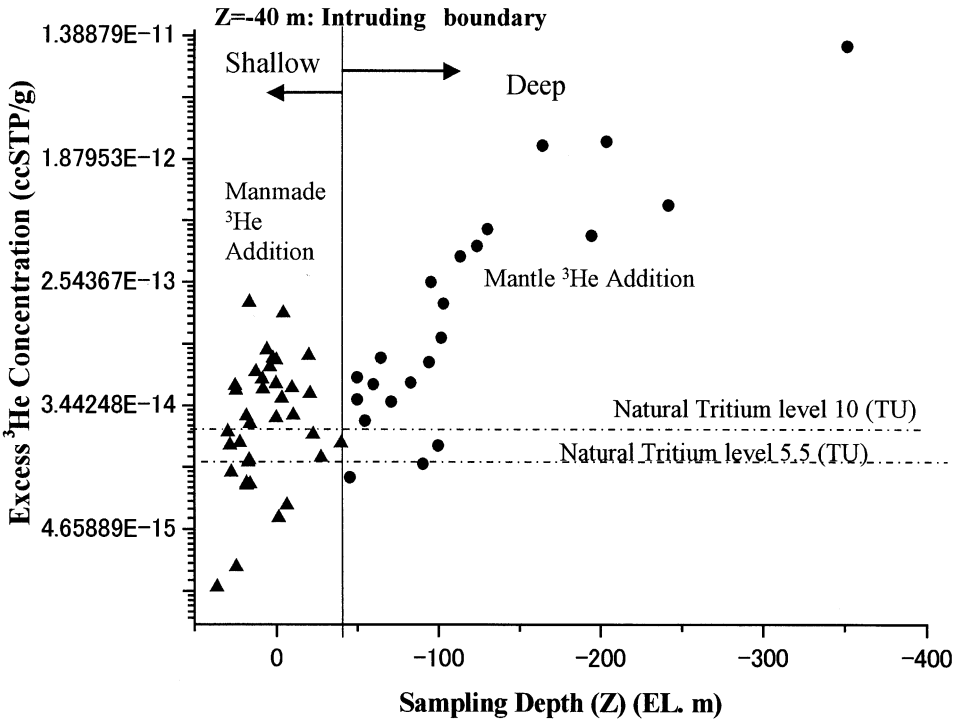

Fig. 3. Relationship between the distribution of excess ^{3}He content in groundwater and the depth of collected groundwater in a borehole. The excess ^{3}He peak in the shallow groundwater zone was derived from tritiogenic ^{3}He, from the beta decay of artificial ^{3}H. In contrast, deep groundwater has accumulated natural ^{3}He from radiogenic He and mantle He. In the calculation of excess ^{3}He content, the ^{3}He content was corrected by Torgersen et al., Torgersen's model (1979) in the event that excess air was contained in the groundwater sample. The solid triangle refers to shallow groundwater collected above 40 m below sea level; the solid circle refers to deep groundwater collected below 40 m below sea level; 5.5 TU ^{3}H level indicates excess ^{3}He contained in groundwater when all ^{3}H turned into ^{3}He by beta decay is stored in groundwater without degassing and diffusing if the natural ^{3}H level is 5.5 TU; 10 TU ^{3}H level: indicates excess ^{3}He contained in groundwater when all ^{3}H turned into ^{3}He by beta decay has been stored in groundwater without degassing and diffusing if the natural ^{3}H level is 10 TU).

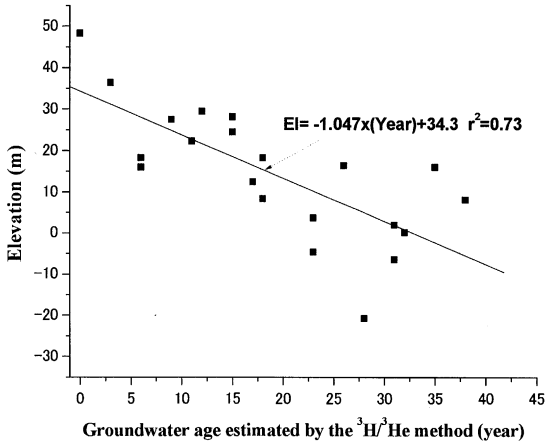

Fig. 4. Groundwater age gradient estimated from the correlation between the ^{3}H/^{3}He ages and sampling depth of groundwater on the tableland (groundwater age gradient: 1.05 m/a a correlation coefficient: 0.73).

authors estimated the residence time of shallow groundwater that lies beneath the tableland at the site using the ^{3}H/^{3}He method in Table 1a and Fig. 4.

Groundwater samples with both a maximum ^{3}He content exceeding 1.82×10^{-13} ccSTP/g and a ^{3}H concentration of 20.8 TU were collected at a depth of 16.4 m above sea level. The groundwater age was estimated to be 26 a by the ^{3}H/^{3}He method (Table 1a). Since the groundwater sample was collected in 1991, 28 a had passed since the ^{3}H bomb pulse reached its peak in 1963. Thus, it was deduced from the estimated groundwater age that the groundwater was recharged in 1965, which was approximately consistent with the period during which rainwater was influenced by the pulse of bomb ^{3}H. Since traces of bomb pulse are found in groundwater at a depth of approximately 16 m above sea level (i.e. 24–36 m deep from the ground surface), a vertical percolation velocity of 0.9–1.4 m/a with a piston flow can be estimated. This estimation from the position of the bomb

pulse was approximately in line with that (1.05 m/a) estimated from the groundwater age gradient shown in Fig. 4. On this basis, groundwater at a depth of 40 m below sea level was probably recharged at least 50 a ago. In other words, groundwater below this depth appears to have been recharged before ^{3}H levels in precipitation were first increased by manmade ^{3}H in the late 1940s.

Excess ^{3}He reached its minimum concentration of 1.07×10^{-14} ccSTP/g at depths from −40 to −50 m. It subsequently increased to the maximum concentration of 1.2×10^{-11} ccSTP/g at −350 m (Fig. 3). The increase in excess ^{3}He content in groundwater at depths below 40 m below sea level was caused by the addition of a mantle He component included in the accumulated crustal He during deep groundwater circulation. Because none of the groundwater samples collected deeper than 50 m below sea level contained ^{3}H, it can be deduced that groundwater below this depth is free from intrusion of shallow groundwater contaminated by manmade ^{3}H. It can be concluded that there is an apparent intrusion boundary between shallow groundwater that controls the groundwater circulation in the tableland and deep groundwater that controls the regional flow. Although more detailed investigations will have to be conducted on the boundary, it can be inferred from the results that a trace amount of natural ^{3}H was left in groundwater below the boundary before manmade ^{3}H was injected in the environment.

It has already been mentioned that shallow groundwater has a significant amount of tritiogenic ^{3}He which raises the ^{3}He/^{4}He ratio above 1.36×10^{-6} (Benson and Krause, 1980). The fitted line shown in Fig. 2a suggests that the dissolved He isotope ratio (^{3}He/^{4}He) was extrapolated to be 1.69×10^{-6}. This value is expected for distilled water with a dissolved He content of 4.68×10^{-8} ccSTP/g and with 1.36×10^{-6} as the ^{3}He/^{4}He ratio after all the ^{3}H at the natural level of 6.2 TU has been converted into tritiogenic ^{3}He (i.e. addition of 1 54×10^{-4} ccSTP/g of ^{3}He). This indicates that groundwater that is only recharged with precipitation with a ^{3}H level of 6.2 TU will have a He isotope ratio (^{3}He/^{4}He) of 1.69×10^{-6}, providing there is no addition of excess He or diffusion loss to the equilibrium atmospheric He content. When we take into consideration the boundary between shallow groundwater and deep groundwater at the depth of 50 m below sea level, this suggests that groundwater at depths greater than 50 m below sea level was recharged before the effects of manmade ^{3}H pushed up the ^{3}H concentration in precipitation.

Although the natural ^{3}H level should change with latitude and the global variation of the intensity of cosmic rays in the long term, this extrapolated result suggests that precipitation in the era before artificial disturbance around this area (at N 42°) contained approximately 6–7 TU as the natural ^{3}H level without degassing and diffusion loss. Unfortunately, there is no way of checking the accuracy of the estimate of the natural ^{3}H production level since no direct measurements of either rainwater or vintage wine were made before 1952 in Japan. Discussions continue about how long-term changes in ^{3}He content can be used to confirm the estimated natural ^{3}H production level.

The degassing loss of ^{3}He in a sedimentary aquifer should not be significant because it is composed of porous media. Osenbrück et al. (1998), for example, reported that the He diffusion coefficient in interstitial water in sedimentary rock was 6.3×10^{-3} m^2/a, which was less than 1/30 of the 1.9×10^{-1} m^2/a in free water (Jahne et al., 1987). Solomon et al. (1993) estimated 47×10^{-2} m^2/a as the effective ^{3}He diffusion coefficient in a silty sand aquifer with a porosity of 30% under groundwater recharge conditions in the tableland. Solomon and Cook (2000), using Schlosser's Eq. (4) (Schlosser et al., 1989), found that the ^{3}He loss in the recharged area was less than 1%, based on a vertical downward velocity of more than 0.5 m/a and recharge rate of 150 mm. Furthermore, Schlosser et al. (1989) reported that more than 75% of ^{3}He was confined to groundwater even in the case of a high dispersion of 1.5 m^2/a with vertical flow velocity above 0.5 m/a. Since the plateau tablelands are a recharge area, and groundwater moves downward with a vertical velocity of 0.9 to 1.4 rn/a at a recharge rate of 300 mm/a, the loss of ^{3}He is negligible if dispersion is at the same level as the 0.047 m^2/a observed by Solomon et al. (1993). Consequently, both the ^{3}He loss from the naturally generated ^{3}H, and the ^{3}He accumulation from mantle He diffused from a deep floor, are negligible around a depth of 50 m below sea level, due to downward groundwater percolation.

Another change in the dissolved ^{3}He concentration is also considered in the estimation of the magnitude of the in-situ production rate of ^{3}H by natural neutron activation in the surrounding rocks. Again, according to Lehmann and Loosli (1991), the natural irradiated ^{3}H level is estimated to be $<8.5\times10^{-6}$ TR/$g_{(water)}a^{-1}$ This ^{3}H production level in the rocks is negligibly small, because there is nothing to add to the 2.1×10^{-20} ccSTP/g a^{-1} of ^{3}He even if all the ^{3}H produced in rocks turned into tritiogenic ^{3}He and was released into the groundwater.

Finally, it can be concluded that in northern Japan the atmospheric natural ^{3}H level would probably be 6 TU in precipitation without bomb effects. This is approximately the same as the 5–7 UT that Kaufman and Libby predicted in 1954 from the data collected in mid-latitude North America and as estimated from the ^{3}H level in European vintage wine samples of the 1920s and 1940s (Clarke and Fritz, 1997). Also, it would be no exaggeration to say that this harmonized with 4 TU estimated by Roether (1967) as a natural ^{3}H concentration before 1952 in Germany. Winter precipitation at this site, which significantly recharges groundwater, is strongly influenced by the Siberian air masses that typi-

cally have the same continental effects as similar air masses in North America and Europe. Kimura (1986) estimated that natural ^3H levels in Japan ranged from 5 to 12 TU in the pre-thermo-nuclear tests age, from the inverse-correlation between ^3H production rate and the number of sunspots.

4.3. Estimation of magnitude of degassing He flux and residence time of deep groundwater

If we try to estimate the residence time of deep groundwater using only the ^4He-accumulation rate, it can be expressed by the following equation:

$$\tau = \frac{^4He_{exe}}{A} \tag{2}$$

$$A = \frac{1-n\rho_{rock}}{n\rho_{water}} \Lambda\left(1.19\times[U]\times10^{-13} + 2.88\times[Th]\times10^{-14}\right) \tag{3}$$

where τ is groundwater residence time, $^4He_{exc}$ is excess ^4He dissolved in groundwater, ρ_w is the density of water, ρ_{rock} is the density of rock, A is the in-situ ^4He production rate (ccSTP/g y^{-1}), Λ is the release factor of ^4He from rocks to groundwater and is assumed to be 1.0 for most rocks, [U] is U content in rock (μ per g), [Th] is Th content of rock (μg per g), and n is the effective porosity of rock.

Groundwater residence time for sample D-8 that contains excess ^4He of 1.55×10^{-5} ccSTP/g, excluding atmospheric ^4He from the total, was calculated to be 13.8 Ma. Since the geological formation containing groundwater is a tertiary layer (5.1–24 Ma), this dating was a considerable overestimation. This was due to the lack of knowledge of the dispersion effect of crustal He.

Helium transport analyses using a two dimensional model have already been done by Stute et al. (1992) for the Great Hungarian Basin, Castro et al. (1998) for the Paris Basin, and Bethke et al. (1999) for the Great Artesian Basin. These analyses were roughly done in order to understand the relations among the magnitude of He degassing flux, the He profiles and groundwater flow on a regional scale. The authors attempted to specify He transport in a detailed 3-dimensional analysis in order to estimate the He dispersion effects. The same techniques that Mahara et al. (2001) applied to He transport analyses at the Äspö site in Sweden are used for estimating the accumulation rate of He in groundwater originating from both the He flux released from deep crust and the in-situ production.

The concentration profile of He dissolved in groundwater was estimated using a He transport model combined with groundwater flow analyses in the detailed geological model shown in Fig. 5. The model employed in this study is a 3-dimensional one, given by the following equation.

For groundwater flow: steady state groundwater flow is governed by Eq. (4):

$$\nabla(K\nabla h) = 0 \tag{4}$$

where, K is the hydraulic conductivity tensor, and h is the hydraulic head. The following boundary conditions

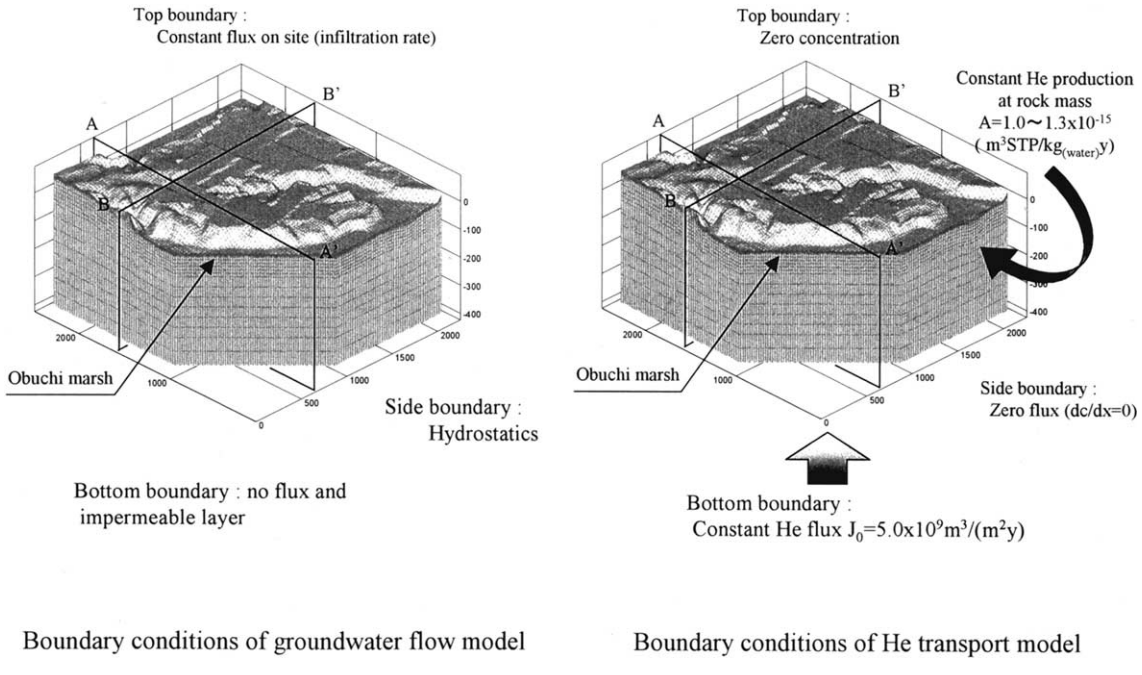

Fig. 5. Schematic figures of analytical models and boundary conditions of groundwater flow and He transport in 3 dimensions.

in the groundwater flow analysis for the He transport analysis using the detailed geological model were assumed: (1) the bottom boundary is a non-flow, in other words $\partial h/\partial n = f(x, y, z)$ which is approximately zero because rock permeability at $< 3.5\times10^{-8}$ cm/s, is extremely low and the hydraulic gradient is negligibly small; (2) vertical boundaries have distributions of in-situ groundwater pressure; and (3) a top boundary gives a net infiltration rate of rainwater observed at the site. The infiltration rate of 300 mm/a was determined by subtracting the evapotranspiration rate of water, estimated by Penmann's method (1948), from the total rainwater precipitated on the site. Furthermore, the representative hydraulic conductivity measured in-situ for each geological layer was used. The distribution of groundwater velocity obtained during the analysis is shown in Fig. 5.

This result indicates that the shallow groundwater, down to a depth of 40 m below sea level, had been circulating with a relatively fast groundwater flow velocity. This is consistent with the observation that the boundary between shallow groundwater and deep groundwater lies under the site. Meanwhile, the average vertical velocity is estimated to be approximately less than 1.4 m/a even in its shallow zone. This result is also supported by the in-situ observation that the groundwater hydraulic conductivity of rock decreases with increasing depth. At this site, the conductivity was observed to decrease by one order for every increase of 200 m in depth.

For He transport:

$$\nabla(D\nabla C - VC) + A = \left(1 + \frac{\rho}{\phi}K_d\right)\frac{\partial C}{\partial t} \quad (5)$$

where C is the excess dissolved He concentration, D is the dispersion coefficient tensor of He, V is the average linear interstitial groundwater velocity, ϕ is the porosity of the stratum, ρ is the bulk density of the stratum, K_d is the He sorption coefficient and is zero in this study, and A is the in-situ production rate of He [ccSTP/g(water)y]. Eq. (5) is rewritten as follows:

$$\nabla(D\nabla C - VC) + A = \frac{\partial C}{\partial t} \quad (6)$$

Table 3 lists in more detail the analytical conditions and parameters used in the groundwater flow analyses and the He transport.

In the He transport analyses, this equation was solved under boundary conditions which have a constant He flux from the bottom boundary, zero flux due to zero gradient of He concentration $D \times \partial C/\partial n = 0$ at vertical boundaries, zero excess He concentration at the ground surface, and in-situ He production rates for each component rock of the analytical area.

To estimate the dispersion effects of He in the stratum, the longitudinal dispersion coefficient should be expressed in terms of $D_L = \alpha_l V + D^*$, where α_l is longitudinal dispersivity, V is the velocity of groundwater and D^* (0.047 m^2/a; Solomon et al., 1993) is the effective diffusion coefficient of He that includes the effects of tortuosity and constrictivity of the porous medium.

The longitudinal dispersivity generally depends on the scale of the site. According to a critical review on field-scale dispersion in both porous media and fracture systems by Gelhar et al. (1992), the longitudinal dispersivity initially increases linearly with distance and approaches a constant asymptotic value. Since the analytical field scale is 2500×2200 m, approximately 100 m should be suitable for the longitudinal dispersivity (Gelhar et al., 1992). The transverse dispersion coefficient is also expressed in terms of $D_T = \alpha_T V + D^*$ by using a transverse dispersivity whose magnitude is less than 1/10 of a longitudinal one (Gelhar et al., 1992). Although further research into the selection of dispersivity will be required, for the purposes of this study, 100 m, 10 m and 0.05 m^2/a as α_L, α_T and D^*, respectively, were used.

Given that the distribution of groundwater flow velocity for the entire study area is known (Fig. 6), the

Table 3
Parameters for analyses of groundwater flow and He transport: setting hydraulic conductivity[a] (m/a) for each geological layer based on data measured in-situ, and the He production rates and degassing flux

Geological formation and depth	From ground level to EL.−50 m	From EL.−50 m to EL. −150 m	From EL.−150 m to EL. −300 m	From EL.−300 m to EL. −400 m	He production rate ($m^3STP/kg_{(water)}a$)
Quatennary	214.0	N.E.[b]	N.E.	N.E.	1.2×10^{-15}
Coarse sandstone	4.34	N.E.	N.E.	N.E.	1.0×10^{-15}
Fine sandstone	2.20	N.E.	N.E.	N.E.	9.7×10^{-16}
Tuffacerous fine sandstone	2.20	1.10	0.09	0.009	9.7×10^{-16}
Pumicetuff	1.94	1.10	0.09	0.009	1.3×10^{-15}
Sandy mudstone	N.E.	0.11	0.09	0.009	1.0×10^{-15}
Mudstone	N.E.	N.E.	0.09	0.009	1.0×10^{-15}

[a] Hydraulic conductivity was set in consideration of conductivity, which drastically decreases as the depth of the geological layer increase. He degassing flux from bottom boundary: $5.0\times^{-9}$ (m^3STP/m^2 a)

[b] N.E.: non-existent.

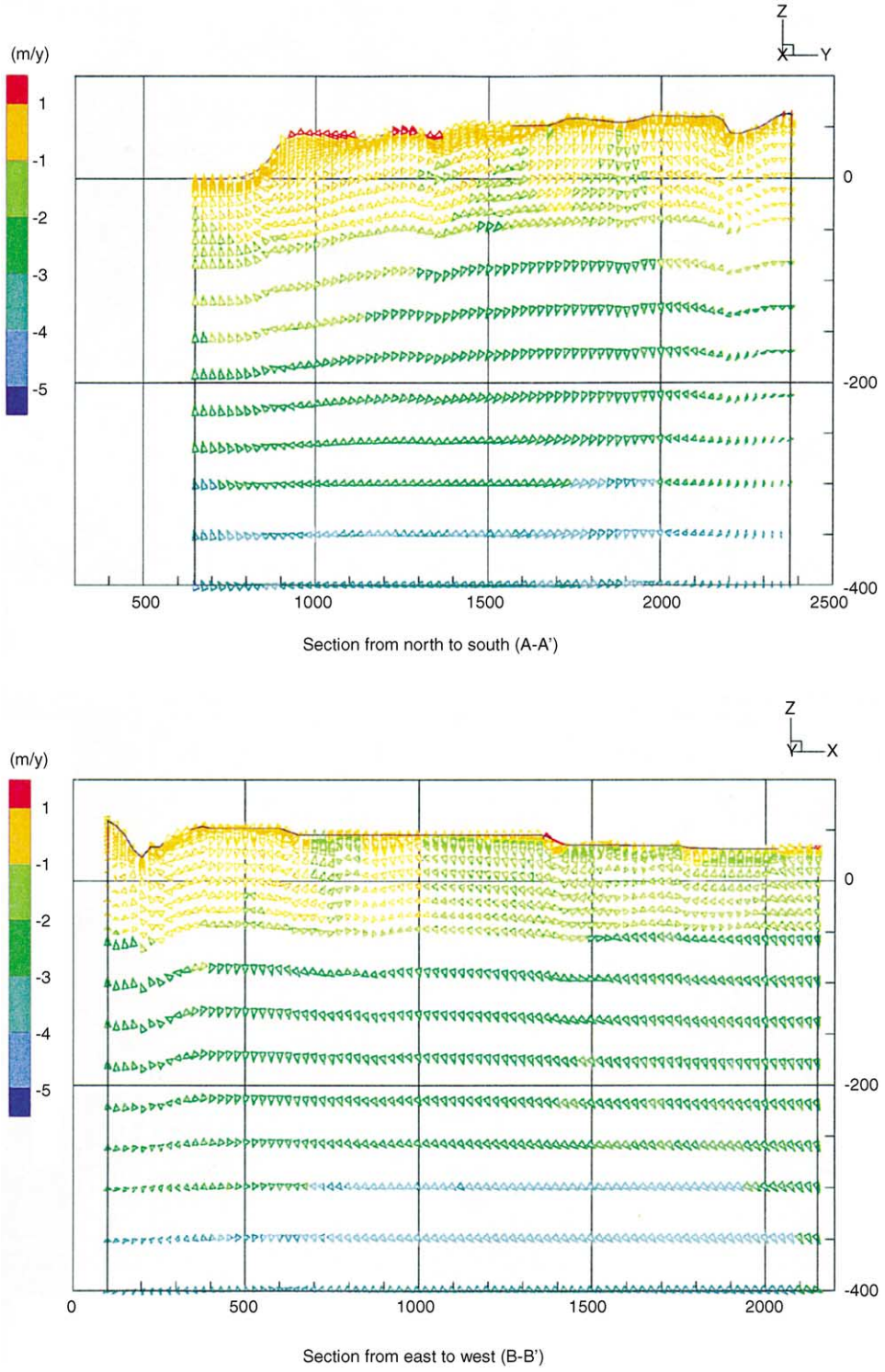

Fig.6. Vertical distributions of the analyzed groundwater velocity at line A–A′, and at line B–B′ shown in Fig. 1.

magnitude of apparent vertical dispersion at the study site can be estimated. The average vertical Darcy velocity decreases drastically with increasing depth. In other words, it is 6.50×10^{-4} m/a at 100 m below sea level, 1.66×10^{-4} m/a at −200 m, 8.36×10^{-5} m/a at −300 m and 1.56×10^{-5} m/a at −400 m, respectively. Therefore, the magnitude of apparent vertical dispersion of He is 5.65×10^{-2} m^2/a at 100m below sea level, 5.02×102^{-2} m^2/a at −200 m, 5.01×10^{-2} m^2/a at −300 m and 5.00×10^{-2} m^2/a at −400 m, respectively.

The magnitude of vertical dispersion is strongly dependent on the effective molecular diffusion coefficient more than 100 m below sea level. This is because the effects of He molecular diffusion in porous media are greater than groundwater flow dispersion effects due to low velocity. The apparent vertical He dispersion coefficients range from 5.0×10^{-2} m^2/a to 5.7×10^{-2} m^2/a at depths greater than 100 m below sea level. Therefore, at this site, the apparent He dispersion effects are in all likelihood controlled by the effective molecular diffusion in groundwater circulation at depths greater than 100 m below sea level.

The magnitude of the He flux, degassing from deep floor toward the ground surface by the groundwater movement and He diffusion, can be estimated by substituting the He concentration gradient and apparent He dispersion coefficient of 5.0×10^{-2} m^2/a into an analogy equation similar to Fick's formula. The He gradient is drawn from the observed He profile as shown in Fig. 7 ($He_{con} = 1.0\times10^{-7} + 1.2\times10^{-8}Z + 1.6\times^{-10}Z^2$ Z: depth m). The magnitude of degassing He flux is roughly estimated to be 5×10^{-9} m^3/m^{2}a (4.25×10^9 atoms m^2 s^{-1}) at a depth of 400 m below sea level. The authors therefore verified the magnitude of the estimated degassing flux by comparing it with the degassing flux in other groundwater basins (Table 2).

The magnitude of the He degassing flux summarized in Table 2 ranges from 0.09×10^{10} to 7.6×10^{10} atoms m^2 s^{-1}. This summary indicates that the degassing flux changes locally and is not constant even in the same basin. The magnitude also depends on differences between the direct measurements and estimations from analyses. This summary suggests that its magnitude depends on differences in tectonics and the hydrogeological structures in the basin, the basin scale and the estimation methods. Consequently, the estimation is fully enclosed in this range. It is in line with the only other degassing flux in Japan, the 9.6×10^9 atoms m^2 s^1 estimated by Sano (1986).

When the 3-dimensional distribution of dissolved He concentration was calculated using a predetermined groundwater velocity, the He flux (J_0) 5×10^{-9} m^{3}STP/m^2 a (4.25×10^9 atoms/m^2 s) from the lower boundary was used. The vertical distribution of calculated He concentration at sections A-A′ and B-B′ (see Fig. 1) are illustrated in Fig. 8. In Fig. 9, the calculated excess He concentrations are compared with actual measurements of excess He concentration made in sampling boring wells, and found to be in good agreement. Furthermore in Fig. 10, the correlation between the magnitude of He degassing flux and He concentration profile confirm the

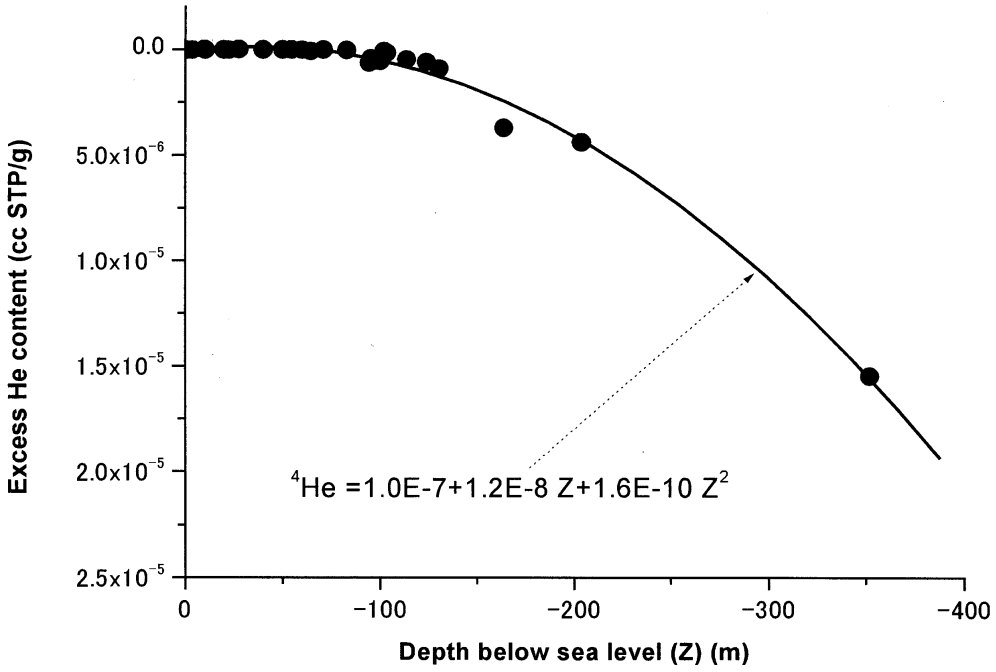

Fig. 7. The He profile showing the correlation between the dissolved He concentration and groundwater sampling depth.

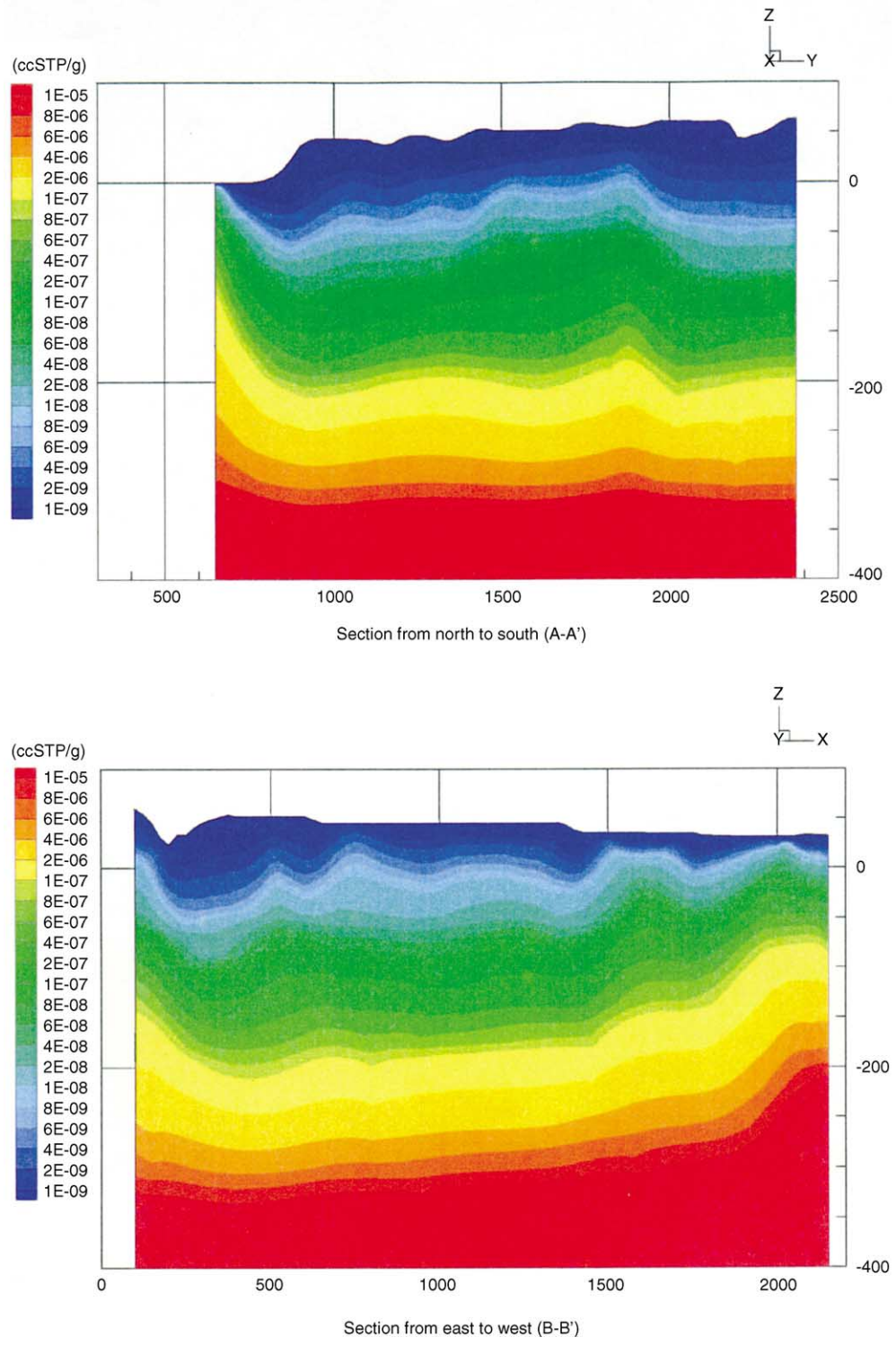

Fig. 8. (1) Vertical contours of He concentration at line A–A′ (global He flux: 5.0×10^{-9} m^3STP/m^2a) in three dimensional analyses, and vertical contours of He concentration at line B–B′ (degassing He flux 50×10^{-9} m^3STP/m^2 a) in 3dimensional analyses (2) Horizontal contours of He concentration at depths of −100,−200,−300 and−400 m (global He flux 5.0×10^{-9} m^3STP/m^2a) in three-dimensional analyses.

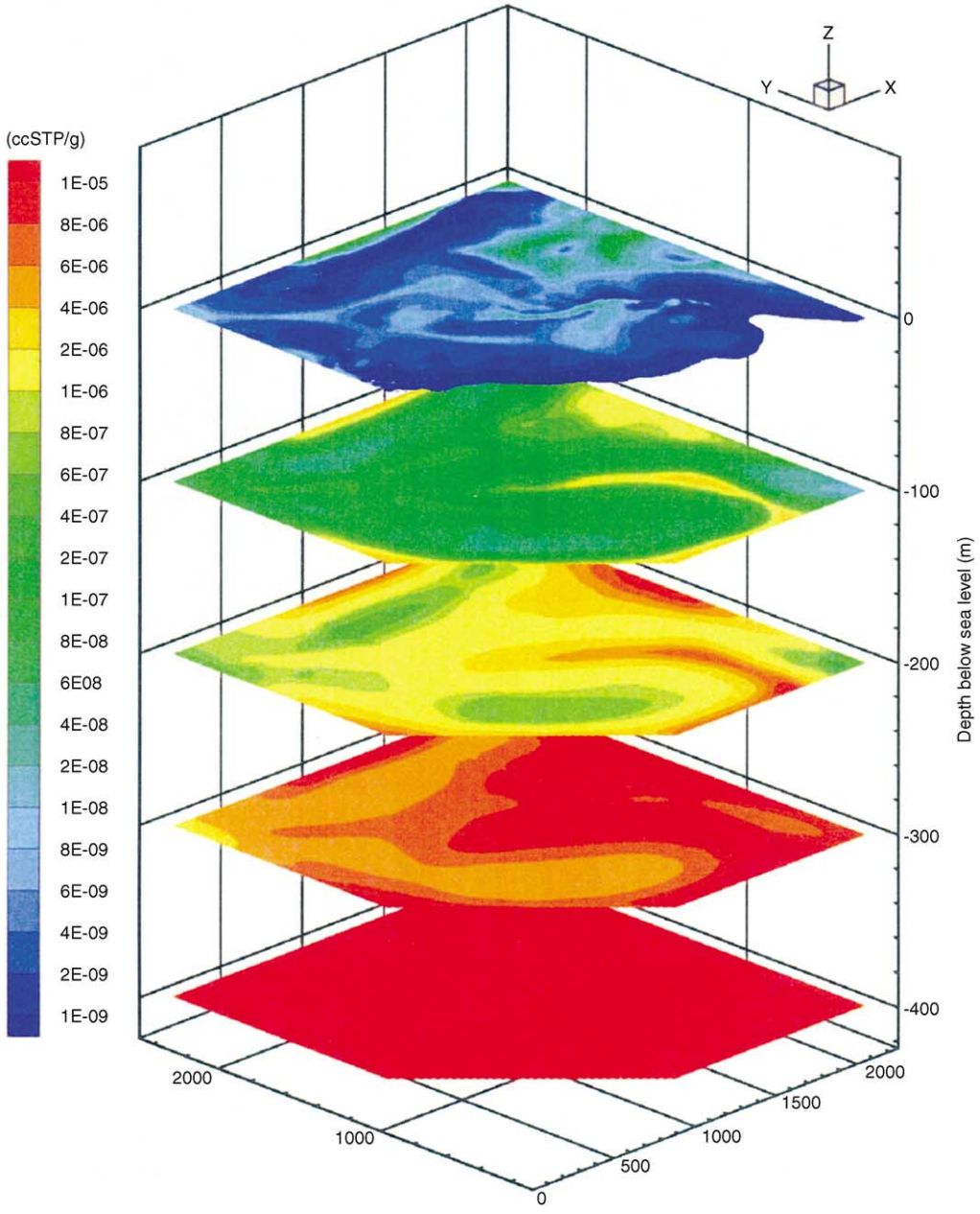

Fig. 8. (*continued*)

practicality of the He flux estimated from the in-situ observation.

The groundwater residence time was estimated using the following equation, which takes into consideration both the effects of vertical dispersion and the in-situ ^{4}He production under a very small vertical groundwater velocity. This is analogous to the methods of Andrews et al. (1985), Weise and Moser (1987), Stute et al., (1992), Osenbruck et al. (1998) and Mahara et al. (2001):

$$T = \frac{\left[{}^4\mathrm{He}\right]_{\mathrm{exc}}}{\frac{J_0}{\rho_{\mathrm{water}}\phi h} + A} \tag{7}$$

$$J_0 = -D_{\mathrm{app}}\rho_{\mathrm{water}}\frac{\partial\left[{}^4\mathrm{He}\right]_{\mathrm{exc}}}{\partial Z} \tag{8}$$

where J_0 is defined by Eq. (8) which expresses the size of ^{4}He transported in groundwater, based on a ^{4}He-disper-

sion analogous to Fick's law. It is described approximately by an apparent diffusion coefficient, which includes the effects of tortuosity and porosity in porous medium, D_{app} and a gradient of ^{4}He concentration measured in a borehole. The layer porosity and the groundwater sampling depth are ϕ and h in Eq. (7), respectively.

Since the in-situ ^{4}He-production rate A in Quaternary and Tertiary sedimentary rocks is usually smaller than the ^{4}He dispersion effect, the term of ^{4}He-production rate is negligible in Eq. (7). Consequently, the groundwater residence time depends on the excess ^{4}He concentration, the magnitude of ^{4}He dispersion based on a gradient of

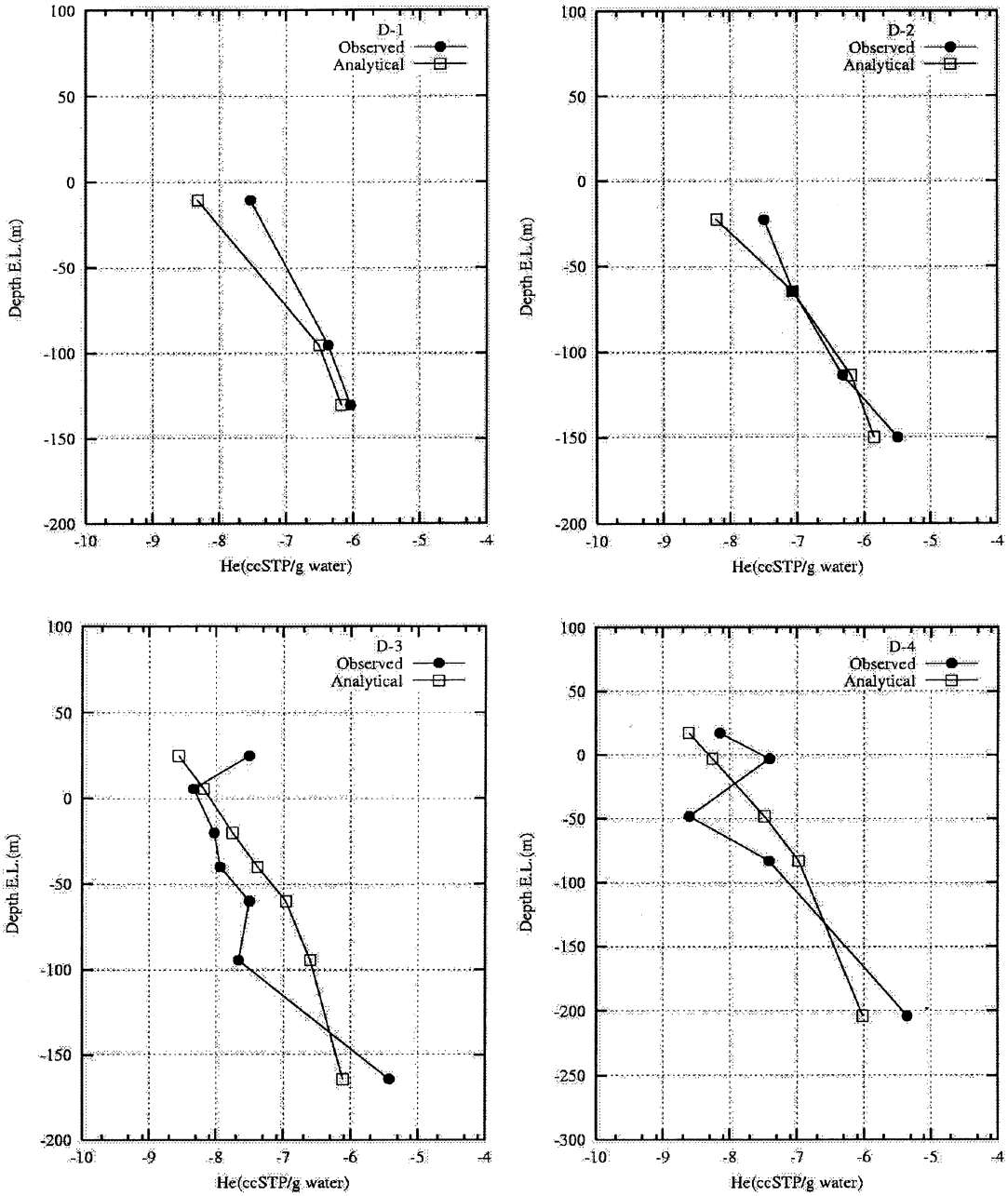

Fig. 9. Comparison between the observed excess He concentration* in deep boreholes (D-1, D-2, D-3, D-4, D-5, D-6, D-7 and D-8) and the analytical result obtained in He transport analyses combined with groundwater flow analyses (solid square: the observed concentration in boreholes; unshaded square: vertical profiles of the ^{4}He concentration dissolved in groundwater analyzed in the He transport model). *Excess He concentration excludes 4.68×10^{-8} ccSTP/g equilibrated with the atmospheric He concentration from the measured He concentration shown in Table 1b.

^{4}He concentration, and the collected groundwater depth.

Empirical in-situ values were substituted for estimated ones in Eqs. (7) and (8): h is a groundwater depth of −352 m, ϕ is 0.44, ρ_{water} and ρ_{rock} are 1.0 and 2.70 g/cm^3, respectively. The in-situ He degassing flux J_0 is 5×10^{-9} m^{3}STP/m$^2_{(water)}$ a, estimated using apparent ^{4}He-diffusion coefficients and the gradient of the He profile. Uranium is 2.7 μg/g, and Th is 7.3 μg/g respectively. Groundwater residence time was estimated to be more than 4.6×10^2 ka for D-8, which was the deepest saline water sample after excluding atmospheric He of 4.68×10^{-4} m/a ccSTP/g from total dissolved He. Other deep groundwater samples collected more than 150 m below sea level also had groundwater residence time of more than 10 Ka. As a cross-check, the turnover time was estimated using the vertical Darcy velocity of 5.9 $\times^{-4}$ m/a, calculated with a hydrologic model at the position of the borehole, −350 m. The Darcy age was

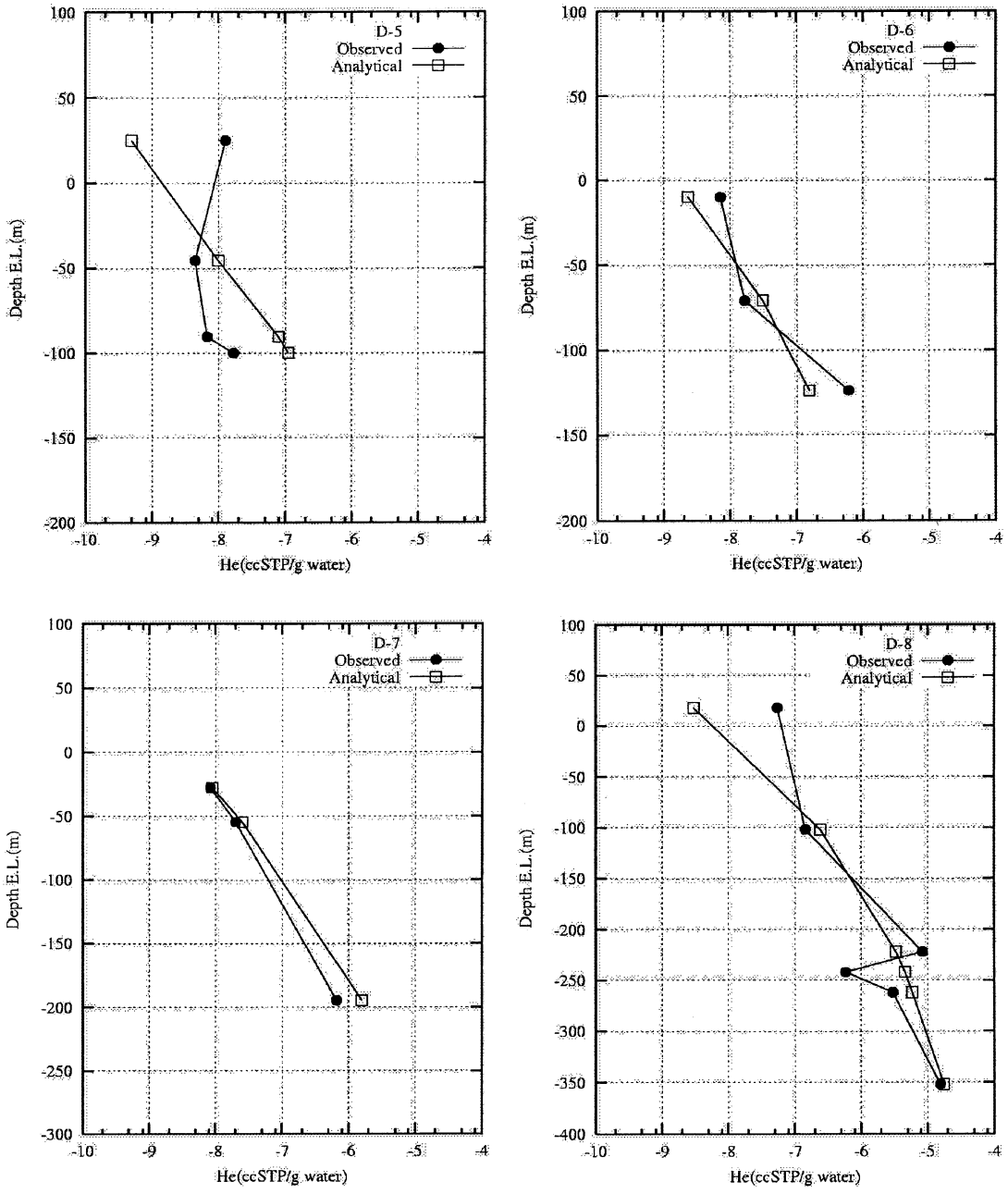

Fig. 9 (*continued*).

estimated to be 5.9×10^2 ka, and is comparable with the He age.

However, analysis of ^{14}C data, sampled in wells bored at this site after 1998, indicates that 2–69% modern C is found in groundwater at depths greater than 150 m below sea level. The modern C level is equivalent to 3–30 ka groundwater residence time. There are significant differences between the He ages and the ^{14}C ages, although both methods were not applied to the same wells. This discrepancy may be caused by the vertical

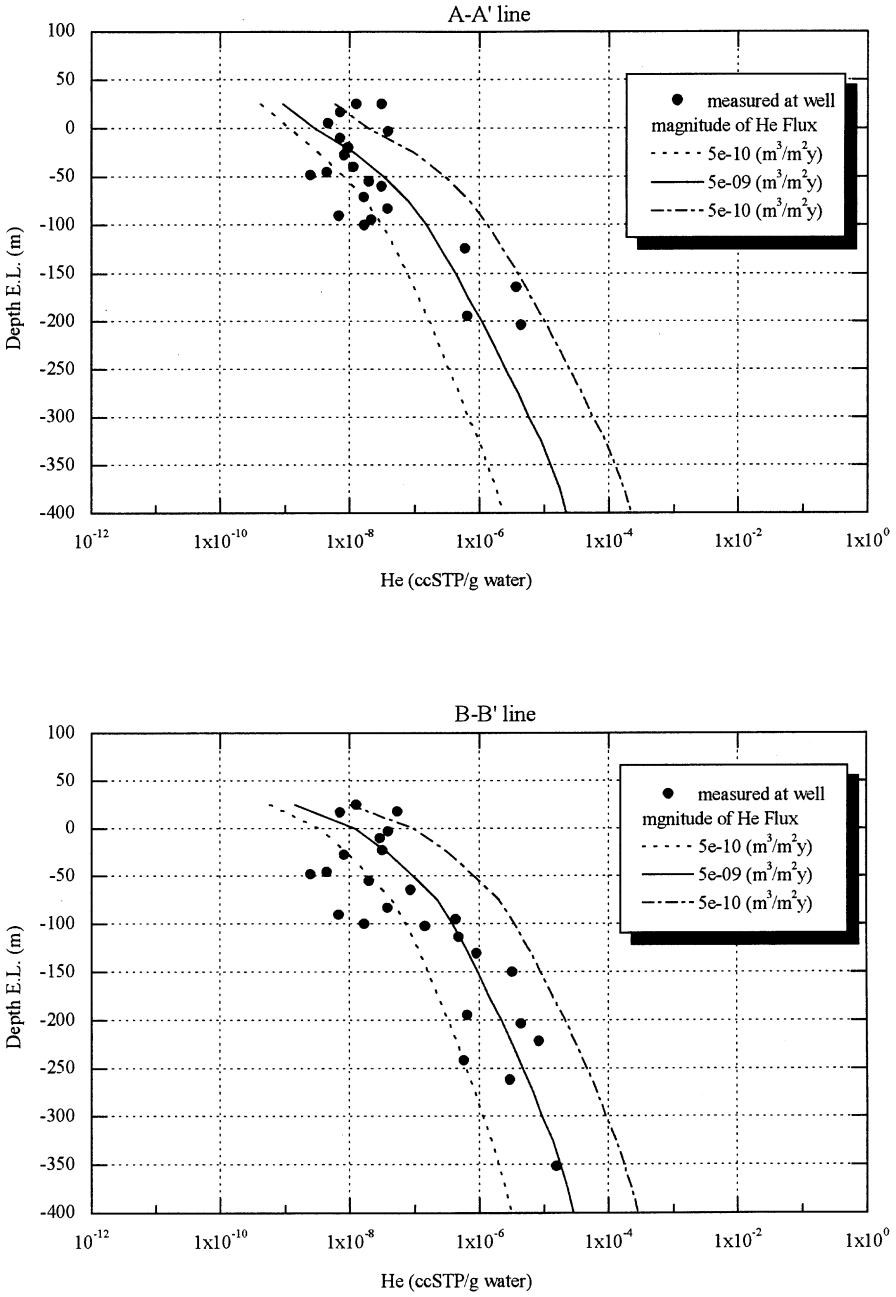

Fig. 10. Comparison between the measured He content and the analytical results, changing the magnitude of the He degassing flux J_0 among 5.0×10^{-10}, 5.0×10^{-9} and 5.0×10^{-8} m^3STP/m^2 a. (The solid square shows He content measured at wells of D-3, D-4, D-5, D-6 and D-7 for the line A–A′, and at wells of D-1, D-2, D-5, D-7 and D-8 for the line B–B′, respectively. Analytical results at lines A–A′ and B–B′ indicate the vertical He content averaged over the entire horizontal axis at lines A–A′ and B–B′ based on He transport analysis.).

disturbance of groundwater during boring and by mixing between young circulating shallow water and very old water stagnating in the pores of sedimentary rock. In order to eliminate this discrepancy, it would be necessary to compare dissolved He concentrations between pore water and groundwater collected from sections in boreholes isolated by a packer system.

5. Conclusion

The conclusions of this study are summarized as follows:

1. The distribution of the tritiogenic ^{3}He peak in the total ^{3}He profile indicates that the intrusion boundary between shallow groundwater (containing man-made ^{3}H) and deep groundwater is 40 m below sea level. The sharp tritiogenic ^{3}He peak indicates the remains of bomb-pulse left in shallow groundwater. Shallow groundwater flow above the intrusion boundary has been controlled by young groundwater recharged with recent rainwater. Shallow groundwater flows downward at a vertical velocity of 0.9–1.4 m/a in the tableland. Meanwhile, deep groundwater flow below the boundary is controlled by older water uncontaminated by manmade ^{3}H.
2. Older, fresh groundwater just below the intrusion boundary was recharged by rainwater with 6.2 TU of natural irradiated ^{3}H level. This suggests that in northern Japan (41 °N) the average natural level of irradiated ^{3}H in rainwater was 6 TU before the increase due to nuclear weapons testing.
3. The degassing He at this site, located close to the fringe of the volcanic front in northern Japan, is composed of crustal He with a ^{3}He/^{4}He ratio of 7.24×10^{-7} that is consistent with of a mixture of 6% mantle He and 94% radiogenic He. The size of the degassing He flux is estimated to be 5×10^{-9} m^3/m^{2}a (4.25×10^9 atoms/m^{2}s) at a depth of 400 m below sea level, which is in line with the only other value estimated in Japan as the degassing He flux.
4. Groundwater more than 150 m below sea level was estimated to be more than 10 ka old. This estimate was based on both the in-situ ^{4}He production rate and the ^{4}He accumulation rate, as determined by Fick's formula using an apparent ^{4}He diffusion coefficient and the gradient of the ^{4}He concentration profile. Discrepancy between the He ages and the MC data suggests that the boring process caused vertical disturbance and that young circulating groundwater mixed with old groundwater that had stagnated in the pores of sedimentary rock.

References

Andrews, J.N., 1992. Mechanisms for noble gas dissolution by groundwaters In: Isotopes of Noble Gases as Tracers in Environmental Studies. IAEA, Vienna, 87–110.

Andrews, J.N., Goldbrunner, J.E., Darling, W.G., Hooker, P.J., Wilson, G.B., Youngman, M.J., Eichinger, L., Rauert, W., Stichler, W., 1985. A radiochemical, hydrochemical and dissolved gas study of groundwaters in the Molasses basin of Upper Austria. Earth Planet. Sci. Lett. 73, 317–332.

Benson, B.B., Krause Jr, D., 1980. Isotope fractionation of He during solution. A probe for the liquid state. J Soln., Chem. 9, 895–909.

Bethke, C.M., Zhao, X., Torgersen, T., 1999. Groundwater flow and the 4He distribution in the Great Artesian Basin of Australia. J. Geophys. Res. 104 (B6), 12999–13011.

Castro, M.C., Goblet, P., Ledoux, E., Violette, S., Marsily, G.d., 1998. Noble gases as natural tracer of water circulation in the Paris Basin 2. Calibration of a groundwater flow model using noble gas isotope data. Water Resour Res. 34, 2467–2483.

Castro, M.C., Stute, M., Schlosser, P., 2000. Comparison of ^{4}He ages and ^{14}C ages in simple aquifer systems: implications for groundwater flow and chronologies. Appl. Geochem. 15, 1137–1167.

Clark, I.D., Fritze, P., 1997. Environmental Isotopes in Hydrogeology. CRC Lewis, New York.

Gelhar, L.W., Welty, C., Rehfeldt, K.R., 1992. A critical review of data field-scale dispersion in aquifers. Water Resour. Res. 28, 1955–1974.

Heaton, T.H.E., 1984. Rates and source of He-4 accumulation in groundwater. Hydrol. Sci. J. 29, 29–47.

Ii, H., Horie, Y., Ishii, T., Shimada, J., 1997. Development of an apparatus to measure groundwater qualities in situ and to sample groundwater using boreholes. Environ. Geol. 32, 17–22.

Jahne, B., Heinz, G., Dietrich, W., 1987. Measurement of the difuusion coefficients of sparingly soluble gases in water. J Geophys. Res. 92 (C10), 10767–10776.

Kaufman, S., Libby, W.F., 1954. The natural distribution of 3H. Phys. Rev. 93, 1337–1344.

Kimura, S., 1986. Behavior analysis of sub surface water using radioisotopes contained in It. Bull. Natl. Res. Inst. Agric. Eng. Japan 25, 1–91. (in Japanese).

Kuroda, T., Katahira, F., Sasaki, T., Imamura, S., 1993. Outline of Rokkasho low-level radioactive waste disposal center and characteristic of bentonite/sand mixtures. Civil Engineering in Japan '93, Japan Society of Civil Engineers 39–58.

Lehmann, B.E., Loosli, H.H., 1991. Isotopes frormed by underground production. In: Pearson Jr, F.J. (Ed.), Applied Isotope Hydrogeology—A Case Study in Northern Switzerland. Studies in Environmental Science. Elsevier, p. 439.

Mahara, Y., 1995. Noble gases dissolved in groundwater in a volcanic aquifer: He isotopes in the Kumamoto plain. Environ. Geol. 25, 215–224.

Mahara, Y., Igarashi, T., Hasegawa, T., Miyakawa, K., Tanaka, Y., Kiho, K., 2001. Dynamic changes in hydrogeochemical conditions caused by tunnel excavation at the Aspo Hard Rock Laboratory (HRL), Sweden. Appl. Geochem. 16, 291–315.

Mattel, D.J., Deák, J., Doveny, P., Horváth, F., O'Nions, R.K., Oxburgh, E.R., Stegena, L., Stute, M., 1989. Leakage of He from the Pannonian basin. Nature 342, 908–912.

Marty, B., Torgersen, T., Meynier, V., 1993. He isotope fluxes and groundwater ages in the Dogger Aquifer, Paris Basin. Water Resour Res. 29, 1025–1035.

Mazor, E., 1972. Paleotemperatures and other hydrological parameters deduced from nobles gases dissolved in groundwaters, Jordan Rift Valley, Israel. Geochim. Cosmochim. Acta 36, 1321–1336.

Mazor, E., Bosch, A., 1992. He as a semi-quantitative tool for groundwater dating in the range of 104–108 years. In:*Isotopes of Noble Gases as Tracers in Environmental Studies* IAEA, Vienna, 163–178.

Osenbrück, K., Lippmann, J., Sonntag, C., 1998. Dating very old pore waters in impermeable rocks by noble gas isotopes. Geochim. Cosmochim. Acta 62, 3041–3045.

Penman, H.L., 1948. Natural evaporation from open water, bare soil, and grass. Proc. R. Soc. London Ser A 193, 120–146.

Ravoire, J., Lorius, C., Robert, J., Roth, E., 1970. 3H content in a firn core from Antarctica. J. Geophys. Res. 75, 2331–2335.

Roether, W., 1967. ^{3}H im Wasserkreislauf. Doctoral dissertation. Univ. Heidelberg (unpublished).

Sano, Y., 1986. He flux from the solid earth. Geochem J. 20, 227–232.

Sano, Y., Wakita, H., 1985. Geographical distribution of ^{3}He/^{4}He ratios in Japan: implications for arc tectonics and incipient magmatism. J. Geophy. Res. 90 (B 10), 8729–8741.

Sano, Y., Wakita, H., 1988. He isotope ratio and heat discharge rate in the Hokkaido Island, Northeast Japan. Geochem. J. 22, 293–303.

Sano, Y, Wakita, H., Hauang, C.-W., 1986. He flux in a continental land area estimated from ^{3}He/^{4}He ratio in northern Taiwan. Nature 323, 55–57.

Sasaki, T., 2000. Study on groundwater permeability in the Neogene sedimentary rock for constructing the disposal system of the low level radioactive waste. Doctoral thesis, Saitama Univ. (in Japanese).

Schlosser, P., Stute, M., Sonntag, C., Munnich, K.O., 1989. Tritiogenic ^{3}He in shallow groundwater. Earth Planet. Sci. Lett. 94, 245–254.

Solomon, D.K., Cook, P.G., 2000. ^{3}H and ^{3}He. In: Cook, P., Herczeg, A.L. (Eds.), Environmental Tracers In Subsurface Hydrology. Klewer Academic Publishers.

Solomon, D.K., Schiff, S.L., Poreda, R.J., Clarke, W.B., 1993. A validation of the ^{3}H/^{3}He method for determining groundwater recharge. Water Resour Res. 29, 2851–2962.

Stute, M., Sonntag, C., Deák, J., Schlosser, P., 1992. He in deep circulating groundwater in the Great Hungarian Plain: flow dynamics and crustal and mantle He fluxes. Geochim. Cosmochim. Acta 56, 2051–2067.

Torgersen, T., 1989. Terrestrial He degassing fluxes and the atmospheric He budget: implications with respect to the degassing processes of continental crust. Chem. Geol. 79, 1–14.

Torgersen, T., Clarke, W.B., 1985. He accumulation in groundwater, I: an evaluation of sources and the continental flux of crustal ^{4}He in the Great Artesian Basin, Australia. Geochim. Cosmochim. Acta 49, 1211–1218.

Torgersen, T., Clarke, W.B., 1987. He accumulation in groundwater, III. Limits on He transfer across the mantle-crust boundary beneath Australia and the magnitude of mantle degassing. Earth Planet. Sci., Lett. 84, 345–355.

Torgersen, T., Clarke, W.B., Jenkins, W.J., 1978. The ^{3}H/He-3 method in hydrology. In Isotope Hydrology Proc Symp 2, 917–930.

Weise, S.M. and Moser, H., 1987 Groundwater dating with He isotopes In:*Techniques in Water Resources Development* IAEA-SM-299/44,Vienna105–126.

Weiss, F.R., 1971. Solubility of He and neon in water and seawater. J. Chem. Eng. Data 16, 235–241.